Giant dipole resonance and Jacobi transition with exact treatment of fluctuations

P. Arumugam,[1,*] G. Shanmugam,[1] and S. K. Patra[2]
[1]*Department of Physics, Manonmaniam Sundaranar University, Tirunelveli–627 012, India*
[2]*Institute of Physics, Sachivalaya Marg, Bhubaneswar–751 005, India*
(Received 13 January 2004; published 21 May 2004)

In a macroscopic approach to giant dipole resonance (GDR) in hot and rotating nuclei, the observables are related to the nuclear free energy surface with consideration of thermal shape fluctuations. This formalism is revisited with more exact methods. The Nilsson-Strutinsky (NS) method extended to high spin and temperature is used for free energy calculations. Various approaches to calculate shell corrections at finite temperature and spin are compared. The GDR built on the states determined by the NS method is studied with a macroscopic model comprising anisotropic harmonic oscillator potential with separable dipole-dipole interaction. Methods to parametrize the free energy, such as the Landau theory, for easier evaluation of thermal fluctuations, are discussed along with a scheme to evaluate thermal fluctuations exactly. The Landau theory is found to work well even in the extreme limits of spin, however, in the absence of strong shell effects. GDR as a probe for Jacobi transition leading to hyperdeformation is analyzed in the case of zirconium isotopes.

DOI: 10.1103/PhysRevC.69.054313 PACS number(s): 24.30.Cz, 21.60.−n, 24.60.Ky

I. INTRODUCTION

The study of structural transitions as a function of both angular momentum and temperature has been among one of the fascinating aspects of highly excited nuclei in recent years [1–4]. The giant dipole resonance (GDR) studies have been proved to be a powerful tool to study such hot and rotating nuclei [5] and recently the domain of GDR spread rapidly over different areas of theoretical and experimental interest. For instance, from the GDR γ decay, it was possible to extract the information of the lifetime of hot superheavy systems such as ^{272}Hs [6]. By populating the isomeric states in the decay of the GDR, better information about the isomers could be extracted [7]. The measurement of GDR gamma rays from highly excited nuclei could be utilized [8] to check the level density prescriptions. In general, the GDR observations provide us information about the geometry as well as the dynamics of nuclei even at extreme limits of temperature (T), spin (I), and isospin (τ). Several experiments have been carried out recently [1–3,9] to study the influence of angular momentum and temperature, by observing the gamma rays from the GDR states from hot rotating nuclei. The behavior of GDR width as a function of temperature has been an interesting phenomenon and the GDR measurements at extreme spins render information about highly deformed structures. In this work we address these two issues with our theoretical results with more exact methods for shell corrections and thermal fluctuations.

In the theory front the microscopic approaches [10,11] (in which GDR can be described as a coherent superposition of particle-hole excitations, often called *p-h* doorway resonance) as well as the macroscopic approaches [12–14] (in which GDR can be coupled to the quadrupole shape degrees of freedom) are successful in explaining most of the GDR features. In the macroscopic approaches, structure of the GDR cross section can be linked with the deformation parameters defining the shape of nuclei. This relation is not straightforward especially in hot nuclei where large-amplitude thermal fluctuations of the nuclear shape play an important role. In this work we employ a macroscopic approach towards GDR with the consideration of thermal fluctuations as well as the quantal fluctuations (shell effects). The theoretical framework thus comprises three parts, namely, (1) a model for nuclear shape calculations that gives the nuclear shape at any given temperature and spin, (2) a model that relates the nuclear shape, at finite temperature and spin, to the GDR cross section, and (3) a formalism that takes care of thermal fluctuations and modifies GDR cross sections accordingly.

After this introduction, in Sec. II we outline the Nilsson-Strutinsky (NS) method extended to finite T and I for calculating the deformation energies. Most of the previous works [13,15] comprise NS calculations extended to finite temperatures without the cranking part. In some works [13,16] shell corrections at finite temperature have been calculated by approximation methods. We revisit the shell correction methods at finite temperature and outline their extension to finite spin. In Sec. III we outline a simple model [17,18] for calculating the GDR width and cross sections at a given T, I, and shape (β, γ). The treatment of thermal fluctuations is discussed in Sec. IV. For time-saving calculations the free energy surface at $I=0\hbar$ were parametrized using the Landau theory [19] and later on an improved parametrization was proposed [14,15]. After outlining the above two methods, we discuss an exact method [20] and bring out the differences between these methods. In Sec.V we present the results of our calculations. First we test our formalism with the results for nuclei for which both experimental and theoretical numbers are reported. The sources of difference/conformity is brought out. Finally we discuss Jacobi transition in Zr isotopes occasionally leading to hyperdeformation. Concluding remarks are laid out in the last section.

*Present address: Institute of Physics, Sachivalaya Marg, Bhubaneswar–751 005, India. Electronic address: aru@iopb.res.in

II. FINITE TEMPERATURE CRANKED NILSSON-STRUTINSKY METHOD

The Strutinsky method of shell corrections [21–23] has been successfully used in calculations of the nuclear deformation energy, with the concept of dividing the total nuclear binding energy into a smooth liquid-drop energy ($E_{\rm LDM}$) and an oscillating shell correction energy (δF),

$$F_{\rm TOT} = E_{\rm LDM} + \sum_{p,n} \delta F. \tag{1}$$

In the case of rotating nuclei the above expression becomes [24]

$$F_{\rm TOT} = E_{\rm LDM} + \sum_{p,n} \delta F + \frac{1}{2}\omega\left(I_{\rm Classical} + \sum_{p,n} \delta I\right). \tag{2}$$

The liquid-drop energy is calculated by summing up the Coulomb and surface energies [25,26] corresponding to a triaxially deformed shape defined by the deformation parameters β and γ. As we are interested in calculating only the relative deformation energies, we neglect the temperature dependence of the liquid-drop parameters whose shape dependence is very weak. The classical part of spin ($I_{\rm Classical}$) is obtained from the rigid-body moment of inertia with surface diffuseness correction [26]. The shell correction is the difference between the deformation energy evaluated with a discrete single-particle spectrum and the deformation energy evaluated with a smooth (averaged) spectrum corresponding to that discrete single-particle spectrum:

$$\delta F = F - \tilde{F}. \tag{3}$$

Similarly the shell correction corresponding to the spin is given by

$$\delta I = I - \tilde{I}. \tag{4}$$

To calculate the shell corrections corresponding to energy and spin, we employ the triaxially deformed Nilsson model together with the Strutinsky prescription. The single-particle energies (e_i) and the spin projections (m_i) are obtained by diagonalizing the triaxial Nilsson Hamiltonian in cylindrical representation [27] up to the first 12 major shells. At finite temperatures the free energy is given by

$$F = \sum_{i=1}^{\infty} e_i n_i - T\sum_{i=1}^{\infty} s_i, \tag{5}$$

where s_i are the single-particle entropy and n_i are the occupation numbers that follow Fermi-Dirac distribution given by

$$n_i = \frac{1}{1 + \exp\left(\dfrac{e_i - \lambda}{T}\right)}. \tag{6}$$

The chemical potential λ is obtained using the constraint $\Sigma_{i=1}^{\infty} n_i = N$, where N is the total number of particles. The total entropy $S = \Sigma_{i=1}^{\infty} s_i$ can be represented in terms of occupation numbers as

$$S = -\sum_{i=1}^{\infty} [n_i \ln n_i - (1 - n_i)\ln(1 - n_i)]. \tag{7}$$

In the following sections we discuss the various methods to evaluate the shell corrections at finite temperature and spin.

A. Numerically exact method

The shell correction is given in terms of the single particle level density as [22,23]

$$\delta F = F - \tilde{F} = \int_{-\infty}^{\lambda} e\, g(e) de - \int_{-\infty}^{\tilde{\lambda}} e\, \tilde{g}(e) de, \tag{8}$$

where $g(e) = d\mathcal{N}(e)/de$ is the single-particle level density and $\mathcal{N}(e)$ is the total number of particles that can be accommodated by the energy levels with their energy $\leqslant e$. λ and $\tilde{\lambda}$ are the chemical potentials corresponding to the discrete and smooth single-particle distributions, respectively. λ and $\tilde{\lambda}$ can be calculated using the constrains $\mathcal{N}(\lambda) = N$ and $\tilde{\mathcal{N}}(\tilde{\lambda}) = N$, respectively. We can also write

$$g(e) = \left.\frac{d\mathcal{N}(\lambda)}{d\lambda}\right|_{\lambda=e} = \sum_{i=1}^{\infty} \left.\frac{dn_i(e_i,\lambda)}{d\lambda}\right|_{\lambda=e}. \tag{9}$$

From Eqs. (6) and (9), we can write the temperature-dependent single-particle level density as [28,29]

$$g(e) = \sum_{i=1}^{\infty} \frac{1}{4T\cosh^2[(e - e_i)/2T]}. \tag{10}$$

The natural way of applying Strutinsky averaging [29] to the level density is to convolute $g(e)$ with the averaging function

$$\tilde{g}(e) = \frac{1}{\gamma_s}\int_{-\infty}^{\infty} \tilde{f}\left(\frac{e - e'}{\gamma_s}\right) g(e') de'. \tag{11}$$

We use the averaging function

$$\tilde{f}(x) = \frac{1}{\sqrt{\pi}} \exp(-x^2) \sum_{m=0}^{p} C_m H_m(x), \tag{12}$$

where $C_m = (-1)^{m/2}/2^m(m/2)!$ if m is even and $C_m = 0$ if m is odd; $x = (e - e_i)/\gamma_s$, γ_s is the smearing parameter satisfying the plateau condition $d\tilde{F}/d\gamma_s = 0$; $p = 6$ is the order of smearing and $H_m(x)$ are the Hermite polynomials.

Substituting Eq. (11) in the expression for $\tilde{F}$ in Eq. (8), and using Eq. (5), we have [28]

$$\tilde{F} = \sum_i e_i \tilde{n}_i - T\sum_i \tilde{s}_i + \gamma_s \int_{-\infty}^{\infty} \tilde{f}(x) x \sum_i n_i(x) dx, \tag{13}$$

where

$$\tilde{n}_i = \int_{-\infty}^{\infty} \tilde{f}(x) n_i(x) dx, \tag{14}$$

$$\tilde{s}_i = \int_{-\infty}^{\infty} \tilde{f}(x) s_i(x) dx. \tag{15}$$

Usually the third term in Eq. (13) is equated to $d\tilde{F}/d\gamma_s$ and can be neglected [29] using the plateau condition. However the inclusion of this term in the calculations leads to a more stable plateau and hence less γ_s-dependent results. The integrals appearing in Eq. (13) are evaluated numerically using the Hermite-Gauss quadrature. Apart from the numerical evaluation of integrals, this method gives exact temperature-dependent shell corrections.

For the spin distribution, the Strutinsky smoothed spin can be derived in a similar way leading to the expression $\tilde{I} = \Sigma_{i=1}^{\infty} m_i \tilde{n}_i$ and hence the shell correction for spin is

$$\delta I = \sum_{i=1}^{\infty} m_i n_i - \sum_{i=1}^{\infty} m_i \tilde{n}_i. \tag{16}$$

B. Maximum term approximation

This method proposed by Civitarese *et al.* [30] provides an approximate solution for the integrals given in Eq. (13) using the "maximum term approximation" of quantum statistical mechanics. The final result of the application of this approximation reads

$$\delta F = E(T) - TS - \tilde{E}(T=0) + \tilde{a}(\lambda_0) T^2, \tag{17}$$

where

$$\tilde{a} = \frac{\pi^2}{6} \tilde{g}(\lambda_0). \tag{18}$$

The term $\tilde{g}$ is given by Eq. (11), which has analytical solution at $T=0$. It is to be noted that in this method there is no need to perform any smoothing at finite temperatures, which is an advantage of this method over the numerically exact method. The shell correction in this approximation is written as

$$\delta I = \sum_{i=1}^{\infty} m_i n_i - \sum_{i=1}^{\infty} m_i \tilde{n}_i, \tag{19}$$

where $\tilde{n}_i$ are evaluated at $T=0$.

C. Cold-nucleus approximation

Starting with the expressions for the smoothed quantities $\tilde{E}=\tilde{a}T^2$ and $\tilde{S}=2\tilde{a}T$, we can write the expression for the smoothed free energy as

$$\tilde{F}(T) = \tilde{E}(T=0) - \tilde{a}T^2. \tag{20}$$

Within the cold-nucleus approximation [19,31], the quantity $\tilde{a}$ is assumed to be shape independent and can be neglected while calculating the relative deformation energy. Hence the smoothed free energy at finite temperature is assumed to be equal to the zero-temperature Strutinsky-smoothed energy, i.e.,

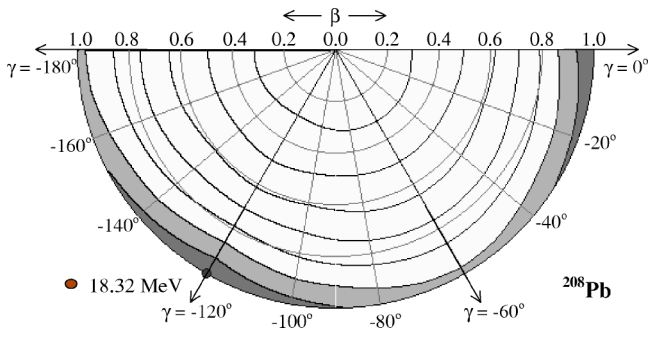

FIG. 1. Shape dependence of $\tilde{a}$ in the nucleus ^{208}Pb. The shaded circle represents the minimum and the contour line spacing is 0.1 MeV.

$$\delta F(T) = F(T) - \tilde{E}(T=0). \tag{21}$$

The difference between this method and the maximum term approximation is the term $\tilde{a}T^2$. To study the shape dependance of $\tilde{a}$, we have plotted in Fig. 1 the contours of $\tilde{a}$ as a function of the deformation parameters for the nucleus ^{208}Pb. From the figure it is clear that the shape dependence is very weak. The difference in free energy due to the term $\tilde{a}T^2$ between the deformations $\beta=0.0$ and $\beta=1.0$ is only around $0.7T^2$. This difference does not have much impact on the equilibrium state but has a role to play in the fluctuation calculations.

D. Statistical method

Ramamurthy *et al.* [32] first identified that the statistical theory can explain the ground state shell corrections. It has been found that the study of variation of S^2 as a function of E^* at asymptotic limits gives information about the smooth (liquid-drop) behavior and, at lower excitation energies, about the shell structure. When one plots these two quantities, it is seen that the curve deviates considerably from a straight line of the form $S^2=4aE^*$, expected from the Fermi gas model. However at excitation energies $E^* > 30-40$ MeV, there exists an asymptotic behavior of the form

$$S^2 = 4a(E^* \pm \Delta E), \tag{22}$$

where ΔE represents the magnitude of the intercepts on the energy axis of the asymptotic straight lines, and ± refers to the two cases of positive and negative shell corrections, respectively. In this framework, after choosing the optimum asymptotic temperature (~4 MeV) we just have to fit a straight line for the asymptotical part of the S^2 vs E^* curve and deduct shell corrections at fixed temperature (or fixed entropy) by simply calculating the difference between the excitation energies given by the actual curve and the fitted line. Shell corrections evaluated in this way are numerically close to the values calculated using the Strutinsky procedure.

In Fig. 2, we present the comparison of shell corrections calculated using different methods for the nucleus ^{208}Pb. From the extension of this calculation to nuclei lying in different mass regions, we have found that both the maximum term approximation method and the statistical method lead to growing positive shell corrections at higher temperatures,

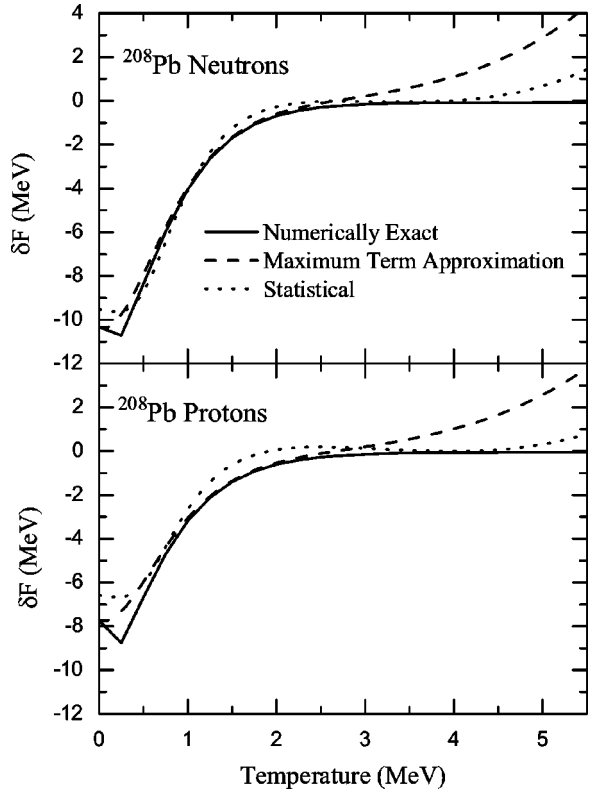

FIG. 2. Comparison of shell corrections calculated using different methods for ^{208}Pb.

which is rather unrealistic. On the other hand, the numerically exact method displays the proper asymptotic behavior, but the results are not stable at very low temperatures ($T<0.5$ MeV) due to numerical instabilities. However this method consumes lot of computing time when compared to other methods. For low mass nuclei, evaluation of shell corrections by the statistical method is found to be less stable. From these arguments we conclude that, for calculating temperature-dependent shell corrections up to ($T\approx 3$ MeV), the maximum term approximation method can be used. At higher temperatures the shell correction term may be neglected or the numerically exact method can be opted.

III. GIANT DIPOLE RESONANCE CROSS SECTIONS

Having discussed the methods to yield deformation energies and hence equilibrium shapes, in this section we briefly outline the model employed in this work for calculating the observables of GDR built on those shapes. In this model the GDR cross sections are obtained using a rotating anisotropic harmonic oscillator potential and a separable dipole-dipole residual interaction [17,18]. The Hamiltonian describing the model is given by

$$H = H_{\rm av} + H_{\rm int}, \tag{23}$$

where $H_{\rm av}$ is the average potential corresponding to the triaxial harmonic oscillator and $H_{\rm int}$ represents the effective dipole interaction:

$$H_{\rm av}(\Omega) = \sum_{\nu=1}^{A} h_\nu(\Omega), \tag{24}$$

where

$$h(\Omega) = \frac{p^2}{2m} + \frac{m}{2}(\omega_x^2 x^2 + \omega_y^2 y^2 + \omega_z^2 z^2) - \Omega\, l_z \tag{25}$$

and

$$L_z = \sum_{\nu=1}^{A} l_z(\nu)$$

is the operator of rotation about the z axis and Ω is the cranking frequency. The effective dipole interaction has the form

$$H_{\rm int} = \eta \sum_{i=x,y,z} \frac{m\omega_i^2}{2A}\left[\sum_{\nu=1}^{A} \tau_3^{(\nu)} x_i(\nu)\right]^2, \tag{26}$$

where $\tau_3^{(\nu)}$ is the third projection of the Pauli isospin matrix and η is a parameter that characterizes the isovector component of the neutron and proton average field. The frequencies of the GDR in a rotating nucleus can be obtained by diagonalizing analytically the Hamiltonian (23) with the effective interaction (26) within the framework of the standard random-phase approximation. Including the splitting of the GDR frequencies due to rotation, the final set of GDR frequencies in laboratory frame are obtained as [17,18]

$$\tilde{\omega}_z = (1+\eta)^{1/2}\omega_z, \tag{27}$$

$$\tilde{\omega}_2 \mp \Omega = \left\{(1+\eta)\frac{\omega_y^2+\omega_x^2}{2} + \Omega^2 + \frac{1}{2}\left[(1+\eta)^2(\omega_y^2-\omega_x^2)^2 + 8\Omega^2(1+\eta)(\omega_y^2+\omega_x^2)\right]^{1/2}\right\}^{1/2} \mp \Omega, \tag{28}$$

$$\tilde{\omega}_3 \mp \Omega = \left\{(1+\eta)\frac{\omega_y^2+\omega_x^2}{2} + \Omega^2 - \frac{1}{2}\left[(1+\eta)^2(\omega_y^2-\omega_x^2)^2 + 8\Omega^2(1+\eta)(\omega_y^2+\omega_x^2)\right]^{1/2}\right\}^{1/2} \mp \Omega. \tag{29}$$

All five of these frequencies do not exist for all nuclei. The number of existing frequencies depends on the shape of the nucleus [18,33]. One can have five GDR components corresponding to the frequencies $\tilde{\omega}_1$, $\tilde{\omega}_2-\Omega$, $\tilde{\omega}_2+\Omega$, $\tilde{\omega}_3-\Omega$, and $\tilde{\omega}_3+\Omega$, for collectively rotating triaxial nuclei. For prolate nuclei ($\omega_x=\omega_y>\omega_z$) rotating about an axis perpendicular to its symmetry axis, all five of the above frequencies will exist. But for the oblate nuclei ($\omega_x=\omega_y<\omega_z$) rotating about its symmetry axis, as shown first by Hilton in Ref. [33], only two frequencies, namely, $\tilde{\omega}_1$ and $\tilde{\omega}_2-\Omega=\tilde{\omega}_3+\Omega$, will exist and thus all effects due to rotation vanish and only those purely due to deformation will be left. For the spherical nuclei ($\omega_x=\omega_y=\omega_z$), which comes under the latter category, one gets only one frequency, namely, $\tilde{\omega}_1=\tilde{\omega}_2-\Omega=\tilde{\omega}_3+\Omega$.

By the semiclassical theory of the interaction of photons with nuclei, the shape of a fundamental resonance in the absorption cross section is that of the Lorentz curve

$$\sigma(E_\gamma) = \sum_i \frac{\sigma_{mi}}{1 + (E_\gamma^2 - E_{mi}^2)^2/E_\gamma^2\Gamma_i^2}, \tag{30}$$

where Lorentz parameters E_m, σ_m, and Γ are the resonance energy, peak cross section, and full width at half maximum, respectively. Here i represents the number of components of the GDR and is determined from the shape of the nucleus. It is to be noted that these Lorentz lines are noninterfering, but Γ_i is assumed to depend on energy. The energy dependence of the GDR width can be approximated by [34]

$$\Gamma_i \approx 0.026 E_i^{1.9}, \tag{31}$$

where E_i are the GDR energies. The peak cross section σ_m is given by

$$\sigma_m = 60 \frac{2}{\pi} \frac{NZ}{A} \frac{1}{\Gamma}\, 0.86(1+\alpha), \tag{32}$$

where α is an adjustable parameter that takes care of the sum rule. The GDR cross-section calculations involve two parameters α and η. The parameter α, which takes care of the sum rule, is fixed at 0.3 for all the nuclei considered in this work. The α has more effect on the peak cross section. In most of the cases as we normalize the peak with the experimental data, the choice of α has less effect on the results. The other parameter η, which denotes the strength of the dipole-dipole interaction, is varied for all the nuclei to obtain the proper ground state GDR centroid energy. The choices are for ^{45}Sc, η=2.1; for ^{90}Zr, ^{92}Mo, and ^{120}Sn, η=2.6; and for ^{194}Hg and ^{208}Pb, η=3.4. For calculating the GDR width, only the power law (31) is used in this work and no ground state width is assumed.

IV. THERMAL AND ORIENTATION FLUCTUATIONS

Fluctuations around mean field values are not negligible in finite nuclear systems [35]. Hence for hot nuclei, instead of calculating the equilibrium values of the observable by minimizing the free energy it would be more appropriate to calculate the expectation value of the observable over the deformation space. This is primarily due to the broadening of free energy landscapes as the free energy distributions no longer show a crisp minimum at finite temperature. When the nucleus is observed at finite excitation energy, the effective GDR cross sections carry information on the relative time scales for shape rearrangements. Hence in the case of hot nuclei, for a meaningful comparison of experimental and theoretical values, the large amplitude thermal fluctuations should be taken care of properly. In the case of hot and rotating nuclei there can be fluctuations in the orientation of the nuclear symmetry axis with respect to the rotation axis. The general expression for the expectation value of an observable $\mathcal{O}$ incorporating both thermal and orientation fluctuations is given by [36]

$$\langle \mathcal{O} \rangle_{\beta,\gamma,\Omega} = \frac{\int \mathcal{D}[\alpha] e^{-F(T,I;\beta,\gamma,\Omega)/T} (\hat{\omega}\cdot\mathcal{I}\cdot\hat{\omega})^{-3/2} \mathcal{O}}{\int \mathcal{D}[\alpha] e^{-F(T,I;\beta,\gamma,\Omega)/T} (\hat{\omega}\cdot\mathcal{I}\cdot\hat{\omega})^{-3/2}}, \tag{33}$$

where $\Omega=(\phi,\theta,\psi)$ are the Euler angles specifying the intrinsic orientation of the system. The quantity $\hat{\omega}\cdot\mathcal{I}\cdot\hat{\omega}$ is the moment of inertia about the rotation axis $\hat{\omega}$ given in terms of the principal moments of inertia $I_{x'x'}$, $I_{y'y'}$, and $I_{z'z'}$ as

$$\hat{\omega}\cdot\mathcal{I}\cdot\hat{\omega} = I_{x'x'} \cos^2\phi \sin^2\theta + I_{y'y'} \sin^2\phi \sin^2\theta + I_{z'z'} \cos^2\theta. \tag{34}$$

The volume element $\mathcal{D}[\alpha]=\beta^4|\sin 3\gamma|\, d\beta\, d\gamma \sin\theta\, d\theta\, d\phi$.

The study of thermal fluctuations by numerical evaluation of Eq. (33) in general requires an exploration of five-dimensional space spanned by the deformation and orientation degrees of freedom, in which a large number of points are required in order to assure sufficient accuracy (especially at finite angular momentum). The corresponding NS calculation for each point consumes much time. Hence some parametrizations were developed to represent the free energy using functions that mimic the behavior of the NS calculation as closely as possible. Two such parametrizations and the exact evaluation are discussed in the following sections.

A. Extended Landau theory

In the Landau theory of phase transitions in nuclei, developed by Alhassid and collaborators [35–37], the free energy is expanded in terms of certain temperature-dependent constants that are to be extracted by fitting with the NS free energy calculations at fixed temperatures by the NS method. Moreover once the fits involving free energy and moment of inertia are made for the nonrotating case, the calculations can be extended macroscopically to high spin states also. Hence this theory offers an economic parametrization to study the hot rotating nuclei. Initially [37,38], the free energy expansion is made up to the fourth power in the deformation parameter β. The extended Landau theory [16,19] includes expansion up to the sixth power of β given by

$$F(T,\omega=0;\beta,\gamma) = F_0 + F_2\beta^2 + F_3\beta^3 \cos 3\gamma + F_4\beta^4 + F_5\beta^5 \cos 3\gamma + F_6^{(1)}\beta^6 + F_6^{(2)}\beta^6 \cos^2 3\gamma + \cdots, \tag{35}$$

where $F_0, F_2, \ldots$ are the temperature-dependent Landau parameters, which are obtained by least square fitting to the free energy surfaces calculated by the NS method. The general expression for moment of inertia $I_{z'z'}$ is given by

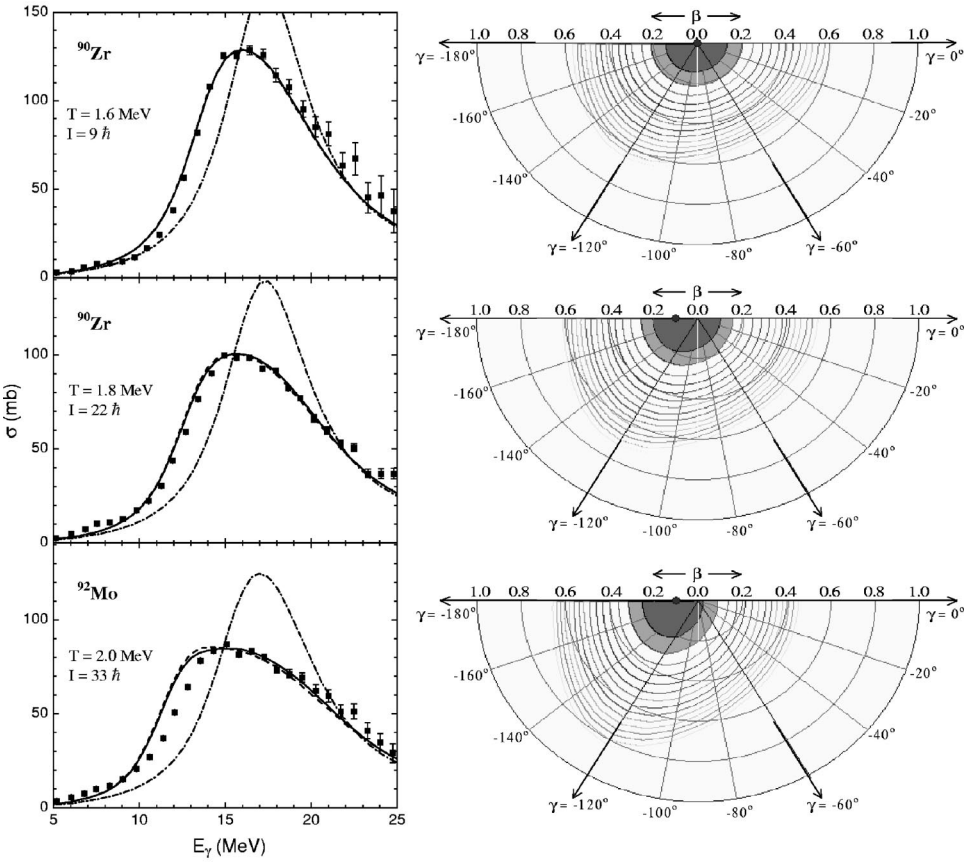

FIG. 3. GDR cross sections and free energy surfaces for the nuclei ^{90}Zr and ^{92}Mo. Left: Experimental data represented by solid squares are taken from Ref. [39]. The solid lines represent calculations with orientation and thermal fluctuations, dashed lines correspond to thermal fluctuations alone, and the dash-dotted lines correspond to most probable shapes. Right: The contour line separation is 0.5 MeV and the most probable shape is represented by a solid circle. The first two minima are shaded.

$$I_{z'z'} = I_0 + I_1 \beta \cos\gamma + I_2^{(1)} \beta^2 + I_2^{(3)} \beta^2 \sin^2\gamma + I_3^{(1)} \beta^3 \cos 3\gamma + I_3^{(2)} \beta^3 \cos\gamma + I_4^{(1)} \beta^4 + I_4^{(2)} \beta^4 \cos 3\gamma \cos\gamma + I_4^{(3)} \beta^4 \sin^2\gamma. \quad (36)$$

The constants $I_0, I_1, \ldots$ are also evaluated using the fitting procedure.

The extended Landau fit for any T and to the second order in ω in terms of the parameters $\alpha_{2\mu}$ (β, γ and Ω) is given by

$$F(T,\omega;\alpha_{2\mu}) = F(T,\omega=0;\beta,\gamma) - \frac{1}{2}(\hat{\omega}\cdot\mathcal{I}\cdot\hat{\omega})\omega^2. \quad (37)$$

It is enough to calculate $I_{z'z'}$ for rotations around a principal axis z' and the other moments of inertia are then given by

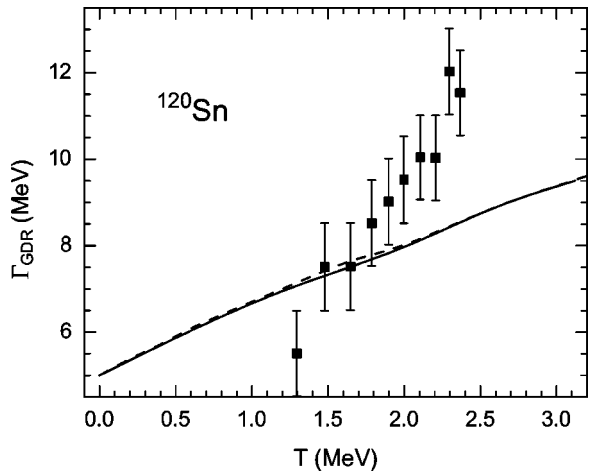

FIG. 4. GDR width at different temperatures for the nucleus ^{120}Sn obtained by NS calculations (solid line), liquid-drop model calculations (dashed line) in comparison with the experimental data points [40] (solid squares).

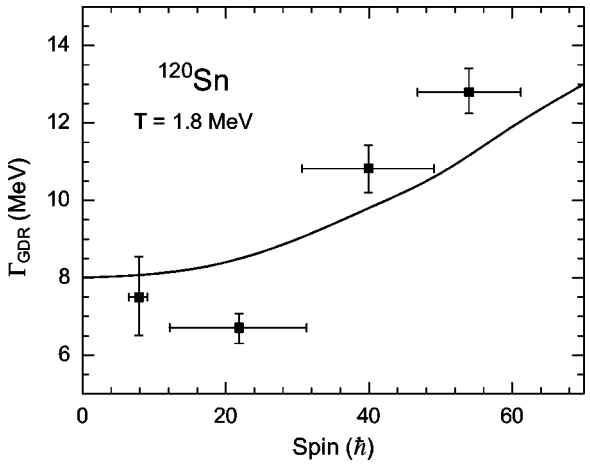

FIG. 5. GDR width at different angular momentum for the nucleus ^{120}Sn. The experimental data points represented by solid squares are taken from Ref. [41]. The theoretical results are represented by the solid line.

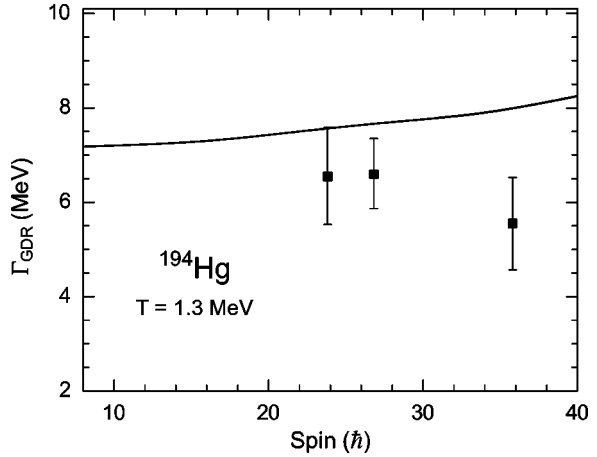

FIG. 6. The GDR width at different spins for the nucleus ^{194}Hg. The experimental GDR widths represented by solid squares are taken from Ref. [42]. The solid line represents our theoretical results.

$$I_{x'x'}(T;\beta,\gamma)=I_{z'z'}(T;\beta,\gamma-2\pi/3),$$

$$I_{y'y'}(T;\beta,\gamma)=I_{z'z'}(T;\beta,\gamma+2\pi/3). \quad (38)$$

In the saddle point approximation the free energy at constant spin is obtained by a Legendre transform [13]

$$F(T,I;\alpha_{2\mu}) = F(T,\omega=0;\beta,\gamma) + \frac{(I+1/2)^2}{2\hat{\omega}\cdot\mathcal{I}\cdot\hat{\omega}}. \quad (39)$$

B. Parametrization of Ormand *et al.*

At larger deformations, it is well known that the NS calculation gives much stiffer free energy. As the Landau theory attempts to combine both the liquid-drop free energy and shell corrections, $\delta F = F - \tilde{F}$, into the same parametrization, the Landau theory is expected to be inadequate. An alternative approach was proposed by Ormand *et al.* [14], in which only the shell corrections are parametrized using a function of rotational invariants. Such a parametrization gives

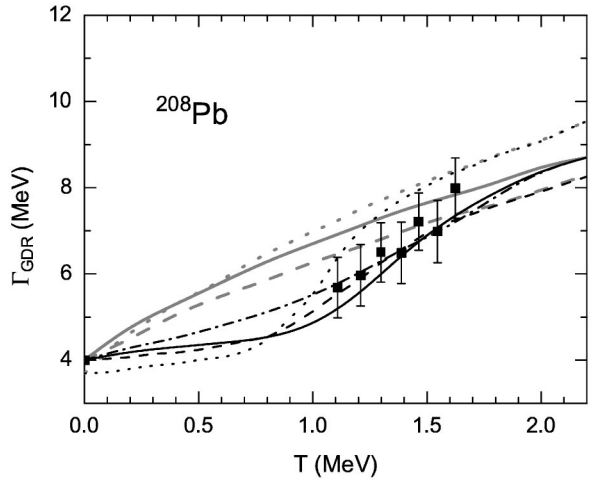

FIG. 7. GDR width at different temperatures for the nucleus ^{208}Pb obtained in present calculations with Landau theory (dash-dotted lines) and exact method (solid lines) in comparison with other theoretical values from Ref. [14] (dashed lines) and Ref. [40] (dotted lines). Black and gray correspond to the NS and liquid-drop calculations, respectively. The experimental data (solid squares) are those from Ref. [40].

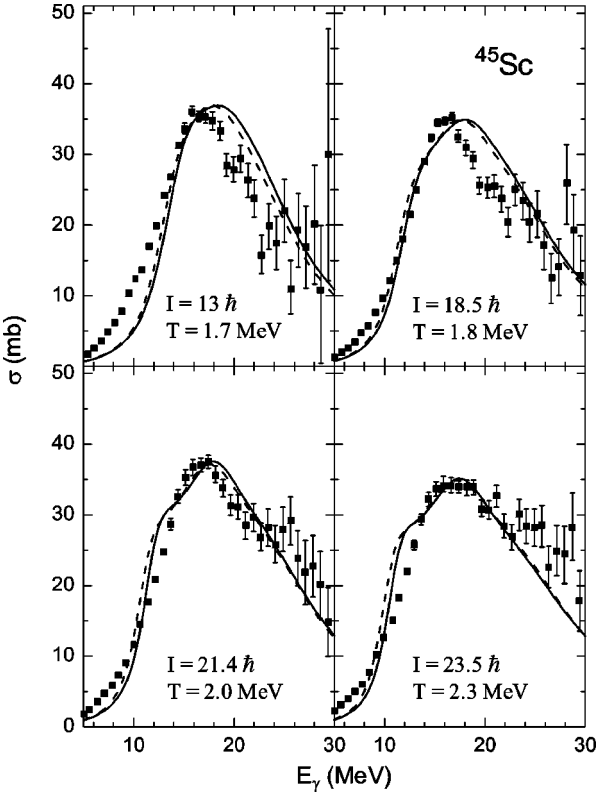

FIG. 8. Comparison between the experimental GDR cross sections in hot ^{45}Sc at different temperatures and spins. The experimental data denoted by solid squares are taken from Ref. [43]. The theoretical results from exact fluctuation calculations are denoted by solid lines and those obtained using Landau theory are denoted by dashed lines.

TABLE I. Jacobi transition in Zr isotopes at $T=0$ MeV.

	Liquid-drop model			Nilsson-Strutinsky		
A	Spin ($\hbar$)	β	γ	Spin ($\hbar$)	β	γ
80	48	0.3	−180	46	0.4	−180
	50	0.5	−140	48	0.8	−120
82	50	0.3	−180	48	0.4	−180
	52	0.5	−140	50	0.9	−120
84	52	0.3	−180	50	0.4	−180
	54	0.5	−140	52	0.9	−120
86	52	0.3	−180	52	0.4	−180
	54	0.5	−140	54	1.0	−120
88	54	0.3	−180	56	0.3	−180
	56	0.5	−140	58	1.0	−120
90	56	0.3	−180	56	0.2	−180
	58	0.5	−140	58	1.0	−120

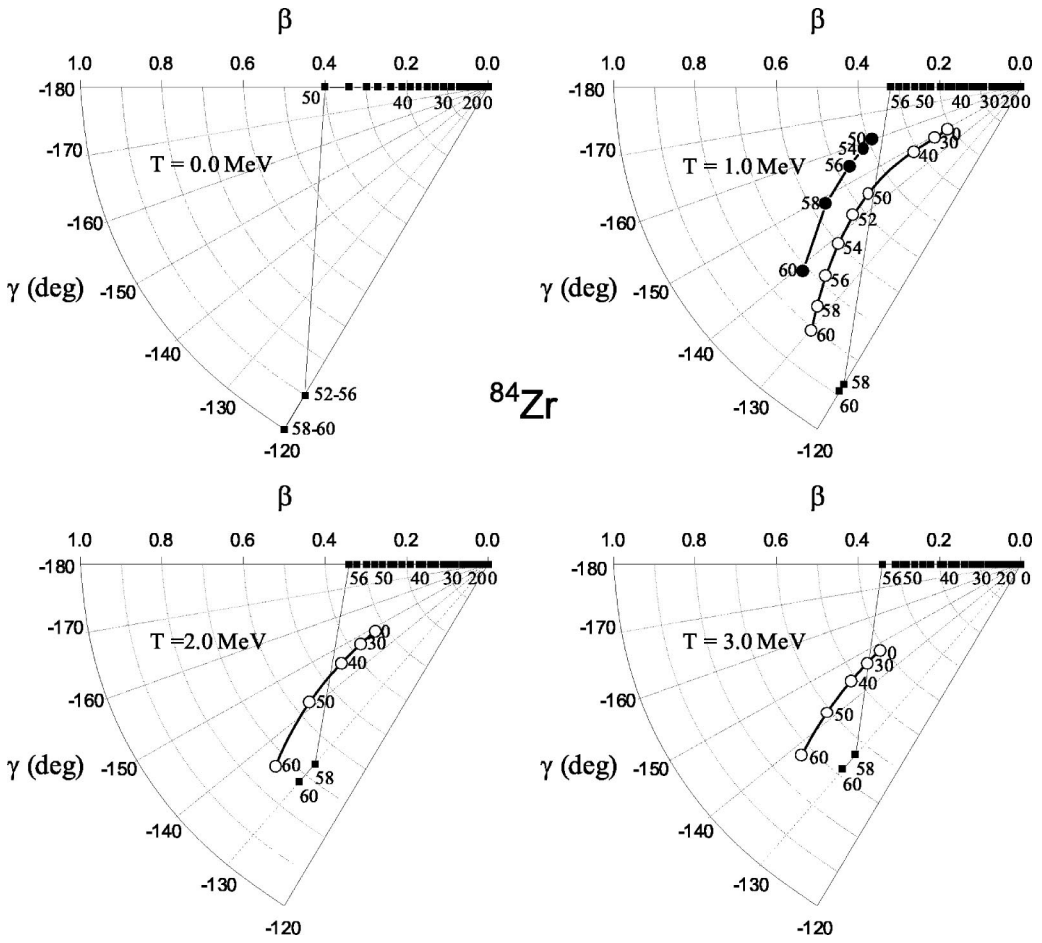

FIG. 9. Hodographs depicting the shape transitions occurring in rapidly rotating ^{84}Zr at different temperatures. The solid squares represent the most probable shapes and the open circle and solid circles represent the thermal averaged shapes calculated with Landau theory and exact method, respectively.

$$\delta F(\beta,\gamma,T) = \sum_{l=0}^{\text{even}} A_l j_l(B_l\beta) C_l T/\sinh(C_l T) + \sum_{l=3}^{\text{odd}} A_l j_l(B_l\beta)\cos(3\gamma) C_l T/\sinh(C_l T), \tag{40}$$

where the j_l are spherical Bessel functions, A_l, B_l, and C_l are obtained by numerical fit to the NS calculations. The shell corrections to the rigid-body moments of inertia were calculated to get the renormalized moment of inertia as

$$\Im = \Im_{\text{rigid}} + \Im_{\text{shell}} - \tilde{\Im} = \Im_{\text{rigid}} + \delta\Im. \tag{41}$$

The parametrization of shell corrections to the moments of inertia gives

$$\delta I_{z'z'}(\beta,\gamma,T) = \sum_{l=0}^{\text{even}} A_l^I j_l(B_l^I\beta) C_l^I T/\sinh(C_l^I T) + \sum_{l=3}^{\text{odd}} A_l^I j_l(B_l^I\beta)\cos(3\gamma) C_l^I T/\sinh(C_l^I T) + \sum_{l\geqslant 1} \alpha_l j_l(\kappa_l\beta)\cos(\gamma + 2\pi/3)\,\eta_l T/\sinh(\eta_l T), \tag{42}$$

where the parameters A_l^I, B_l^I, C_l^I, α_l, κ_l, and η_l were determined by numerical fit to the NS calculations. The free energy for rotating nuclei are calculated using the expressions (37)–(39).

C. Exact fluctuation calculations

With advanced computing systems, nowadays it is possible to perform the thermal fluctuation calculations exactly by numerically computing the integrations in Eq. (33) with the free energies, moments of inertia, and the observables calculated exactly at the deformations corresponding to the integration (mesh) points. In this work we have performed

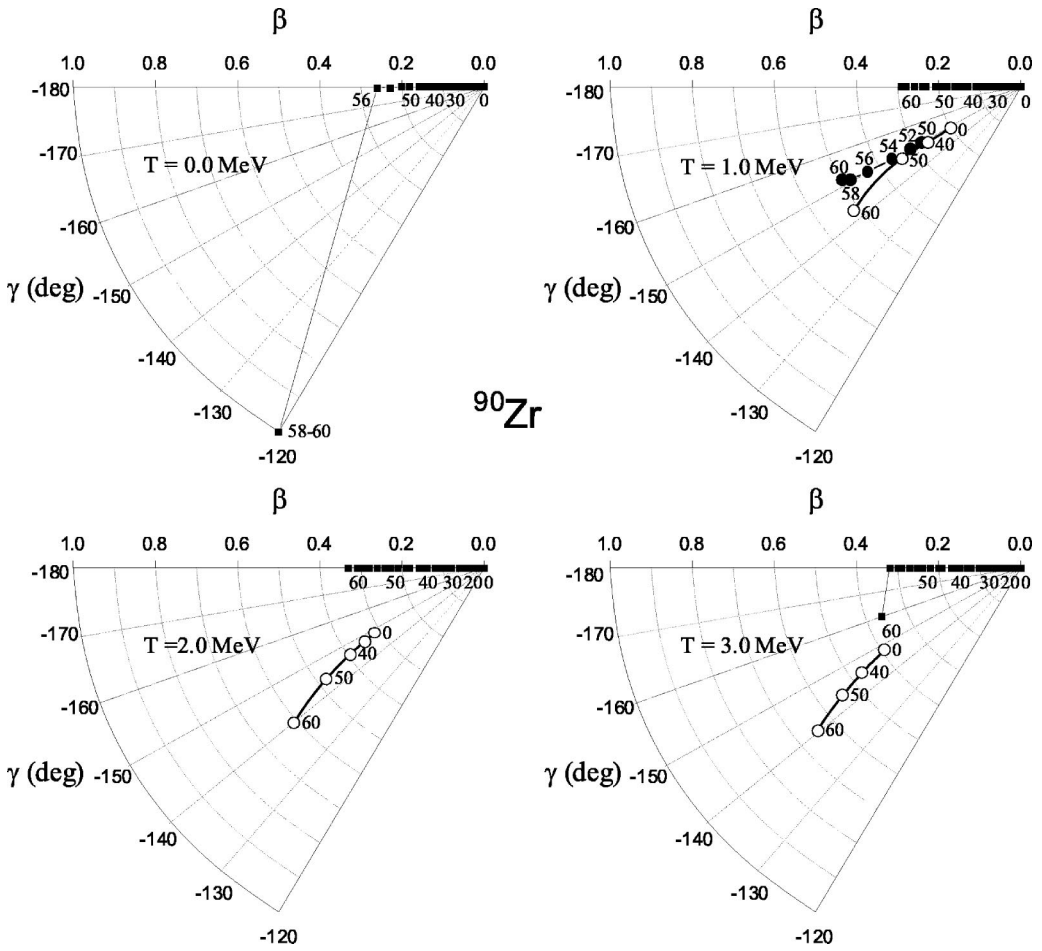

FIG. 10. Same as Fig. 9, but for the nucleus ^{90}Zr.

such calculations, however, neglecting the orientation fluctuations. This enables us to perform the integration in the deformation space only, which at present is two dimensional, having the deformation parameters β and γ. We first compute the free energies at fixed spin and temperature by varying the deformation corresponding to the integration points. We perform a 32-point Gaussian quadrature and hence for one spin and one temperature 32×32 free energies should be calculated by the NS method and stored. Then we perform the integration involving any observable such as σ at different GDR gamma energies. While performing fluctuation calculations in this way, the free energy, GDR cross section, and width at any given spin are obtained by tuning the cranking frequency to get the desired spin. Comparison of results from this procedure and those obtained using the extended Landau theory are presented in the next section.

V. RESULTS AND DISCUSSION

In Fig. 3 we show for the hot rotating ^{90}Zr and ^{92}Mo nuclei, the results of our GDR cross-section calculations along with the experimental results [39]. The free energy surfaces on which the GDR calculations are built have been shown in the right panel. The most probable shapes and thermally averaged shapes evaluated by us [20] at the shown temperature and spin using the Landau theory are consistent with those reported earlier [36] and hence justify our formalism. The increase in the noncollective oblate shape with the spin resembles the behavior of a rotating liquid drop that can also be inferred from the potential energy surfaces. Similar to previous observations [36], from Fig. 3, we see that the thermal fluctuations play a crucial role whereas the orientation fluctuations are negligible while calculating the GDR cross sections. This is true for most of the cases considered here and justify our omission of orientation fluctuations in the exact method. The significant finding [20] in these cases is that the results of the thermal fluctuation calculations using the macroscopic extended Landau theory and the present exact approach are exactly similar (they exactly overlap in Fig. 3). However the Landau theory results are found [20] to deviate from the exact calculations at $T=0.5$ MeV for the nucleus ^{92}Mo and these deviations are attributed to the shell effects driven by the spin. The Landau theory or the later parametrization [14] could not account for these shell effects, which can vary with spin. In both methods the free energy at finite spin is obtained from the free energy and moment of inertia at $I=0\hbar$ using Eq. (39).

To examine GDR widths at high spins we study them in ^{120}Sn, where the GDR widths have been extracted experimentally. In Fig. 4, we show the comparison between the theoretical and experimental widths for the nucleus ^{120}Sn. In

this nucleus the shell corrections from protons and neutrons more or less cancel each other and hence the NS calculation and the liquid-drop model calculations lead to similar results. The overall fit is good and the increase in discrepancy with the increase in temperature may be due to the domination of particle evaporation widths at higher temperatures [14], whose contributions are not taken care of in the present calculations. It has to be noted that the comparison of GDR width from experiment and theory does not require any normalization. In the case of ^{120}Sn also the results of Landau theory and exact fluctuation calculations are found to be exactly similar. To examine this similarity at high spins we have performed a case study with ^{120}Sn and ^{194}Hg for which experimental widths are extracted [41,42] as a function of spin at fixed temperature. The results are shown in Figs. 5 and 6. Again the results of Landau theory were found to be exactly similar to the results of exact calculations. These calculations are very much in accordance with experiment.

In Fig. 7 we show the calculated GDR widths of ^{208}Pb along with other theoretical and experimental results. The presence of strong shell corrections for spherical shape results in large difference in the deformation energies between spherical and deformed configurations. This leads to attenuation of thermal fluctuations at lower temperature and hence we get widths that are much lower than liquid-drop calculations [14]. In the presence of strong shell effects at lower temperatures, the Landau theory results deviate from the results of the exact method [20]. Above $T \sim 1.5$ the results from the two methods are the same. Hence it is clear that the parametrization of the Landau theory is good enough to explain the GDR properties of hot rotating nuclei only in the absence of strong shell effects. It is well known that at larger deformations, the free energy obtained by the Landau theory deviates from the NS calculations [14]. Such differences are suppressed at higher temperatures due to the weakening of shell effects and the thermal fluctuations. In Fig. 7 we have plotted also the reported results [40] from the Landau theory calculations (with cold-nucleus approximation to evaluate shell corrections) as well as the results of Ormand *et al.* (with proper treatment of shell corrections and improved parametrization). The difference in the results from the liquid-drop model clearly suggest that the major part of the difference comes through the different methods adopted for calculating GDR properties rather than the different parametrizations used to deal thermal fluctuations or the proper treatment of shell corrections. The other part of the difference can be ascribed to the variation in liquid-drop parametrizations.

In the region of critical spin also we test our formalism by applying it to explain the Jacobi transition in the nucleus ^{45}Sc, which is established by experiment [43] and theory [44]. Jacobi transition is a sudden phase transition occurring at high angular momentum leading to a transition from a noncollective oblate shape to a triaxial collective shape, which is close to a prolate shape. This transition is analogous to the Jacobi transition occurring in gravitating rotating stars [25]. In Ref. [44] it has been argued that if the Jacobi transition is not assumed, the calculations do not agree with the experiment and hence the Jacobi transition could exist in the case of ^{45}Sc. Our present calculations also give good fit to the experimental data as shown in Fig. 8, supporting the existence of Jacobi transition. To enable comparison with experimental data the GDR cross sections are calculated for an average temperature and spin using the spin distribution given in Ref. [44]. From the results shown in Fig. 8, the ability of the present theoretical formalism to explain the experimental data is justified. Moreover, we can see that even at critical spins, the Landau theory does well in par with the exact calculations. It has to be noted that the marginal difference in the cross sections from these two methods is well quenched while calculating the widths.

From the first identification of Jacobi transition in the finite nucleus ^{45}Sc, several theoretical and experimental investigations [13,26,45,46] were undertaken to survey the existence of this phenomenon in other nuclei. With the availability of new experimental facilities these studies have gathered momentum recently. From our calculations, we have identified [47] the Zr region to be a fertile region to detect Jacobi transition, which can lead to very highly deformed nuclei, such as hyperdeformed nuclei. In Table I we present the results of our calculations at $T=0$ MeV for Zr isotopes with $80 \leqslant A \leqslant 90$. From the results of NS calculations it can be seen that in most of the cases the Jacobi transition leads to hyperdeformation. It is interesting to see that even though the liquid-drop model (LDM) predicts Jacobi transition it does not give rise to hyperdeformation in these cases. For example, in ^{80}Zr the LDM calculations show the Jacobi transition occurring at spin $48\hbar$ to $50\hbar$ changing the deformation β from 0.3 to 0.5. However, the NS calculations predict Jacobi transition in ^{80}Zr altered by spin $2\hbar$ and changes the deformation β from 0.4 to 0.8. In the case of ^{90}Zr the LDM predicts a critical spin $56\hbar$ with β changing from 0.3 to 0.6. The NS calculations predict the critical spin to be $56\hbar$ and the change in deformation β to be 0.2 to 1.0. Hence the quantal fluctuations strongly modify the deformation of the nuclei during the Jacobi transition. However the critical spin at which the transition takes place is marginally affected. These are the observations at cold status ($T=0$ MeV). It is interesting to see whether the Jacobi transition and the hyperdeformed structures survive thermal fluctuations at higher temperatures. From our present theoretical analysis we infer that the hyperdeformed structures in the Zr isotopes considered here do not survive high temperatures. In Figs. 9 and 10 we show the hodographs at different temperatures for the nuclei ^{84}Zr and ^{90}Zr to represent the scenario. The most probable shapes and thermally averaged shapes are shown in the above-mentioned plots. At $T=1$ MeV the averaged shapes at high spins calculated using the NS method are compared with the Landau theory results. The shell effects still dominate at $T=1$ MeV and lead to the difference between the results of the Landau theory and the exact method. This difference is washed out at high temperatures. Apart from suppressing the sharpness of Jacobi transition, the thermal fluctuations do not favor hyperdeformed states.

This can be understood if we consider hyperdeformation as a manifestation of shell effects at high spins. As the temperature increases the shell effects melt and one should expect the liquid-drop behavior. It is interesting to see that the Jacobi transition, which was assisted by shell effects at $T=0$ MeV in ^{90}Zr, seems to be strongly attenuated by the thermal effects. The indication for Jacobi transition can be seen

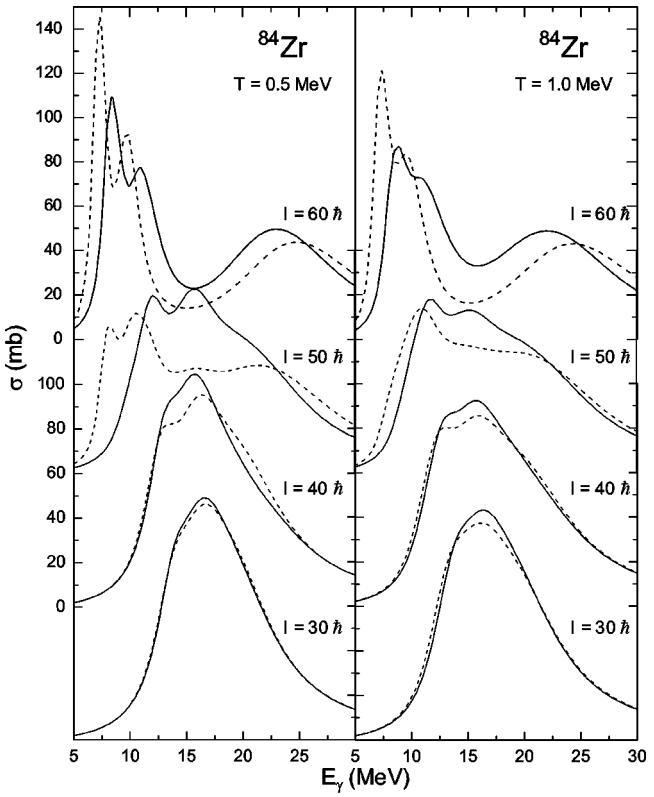

FIG. 11. Theoretical GDR cross sections for the nucleus ^{84}Zr at $T=0.5$ MeV and $T=1.0$ MeV using the Landau theory (dashed lines) and exact method (solid lines) for thermal fluctuations. The existence of the Jacobi transition is clearly seen from the magnitude of splitting.

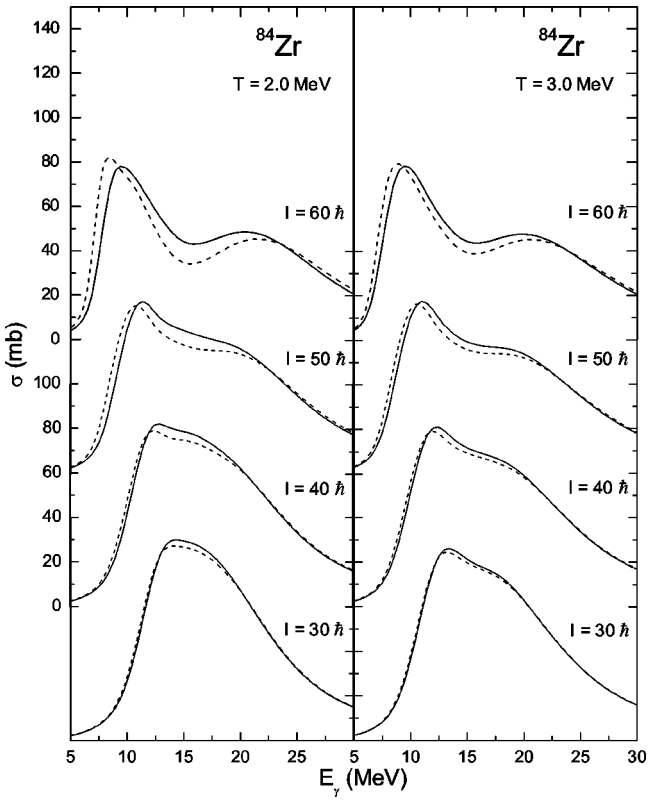

FIG. 12. Same as Fig. 11 but at $T=2.0$ MeV and $T=3.0$ MeV.

in this nucleus only at high temperatures where the shell corrections would have started vanishing. To see how the shell effects are reflected in the GDR cross sections, we present the GDR cross sections in Figs. 11 and 12, which could explain the situation at high temperatures also. The theoretical GDR cross sections for ^{84}Zr at high temperatures and spin clearly depict that there is a strong splitting in the GDR peaks at high spins, which is even stronger than it was in the case of ^{45}Sc. As the shell effects play a vital role in leading to a hyperdeformed shape at low temperatures and at very high spins ($50-60\hbar$), we see the Landau theory results deviating considerably from the exact calculations at very high spins. In these situations, the Landau theory seems to overestimate the width of the GDR. This discrepancy vanishes with the vanishing shell corrections at higher temperatures. In the exact calculations at $T=0.5$ MeV, the averaged deformation parameters $(\bar{\beta},\bar{\gamma})$ during the transition from $I=58\hbar$ to $60\hbar$ change from $(0.42,-156.2°)$ to $(0.88,-129.4°)$. This hints at the existence of Jacobi transition leading to hyperdeformation even in hot nuclei. This transition is well reflected in the GDR cross sections also (Fig. 11) by the strong splitting of the GDR peaks. This splitting, even though attenuated, is present at higher temperatures. Hence the highly deformed shape following Jacobi transition is expected to survive higher temperatures but it may not lead to hyperdeformed shapes. The low temperature ($T\lesssim 1.0$ MeV) GDR measurements are expected to reveal the presence of hyperdeformation.

VI. CONCLUSIONS

In this work we have presented in detail our theoretical framework to study the GDR properties at finite temperature and spin. Shell effects causing the quantal fluctuations are treated with exact temperature and spin dependence. Thermal fluctuations are dealt in an exact way without any parameter fitting. Comparison of our present approach with other similar approaches, like the thermal fluctuation models comprising Landau theory and the parametrization of Ormand *et al.*, has been brought out. We have carried out a systematic study of the GDR properties in the nuclei ^{45}Sc, ^{90}Zr, ^{92}Mo, ^{120}Sn, ^{194}Hg, and ^{208}Pb, and our results are well in conformity with experimental results. The Landau theory is found to be good enough to explain GDR properties, even at very high spins, in the absence of strong shell effects. We have identified the zirconium region as a very fertile region to detect Jacobi transition. At lower temperatures the Jacobi transition leads to hyperdeformation in proton-rich zirconium isotopes. Even though the Jacobi transition survives higher temperatures, it may not lead to hyperdeformation.

ACKNOWLEDGMENTS

We thank A. Ansari and N. D. Dang for their suggestions. One of the authors (P.A.) acknowledges financial support from the Council of Scientific and Industrial Research, Government of India under the scheme CSIR-SRF:9/652(10)/2002-EMR-I.

[1] P. Heckman *et al.*, Phys. Lett. B **555**, 43 (2003).
[2] F. Camera *et al.*, Phys. Lett. B **560**, 155 (2003).
[3] A. Bracco, Acta Phys. Pol. B **34**, 2163 (2003).
[4] D. Kusnezov and W. E. Ormand, Phys. Rev. Lett. **90**, 042501 (2003).
[5] K. A. Snover, Annu. Rev. Nucl. Part. Sci. **36**, 545 (1986); J. J. Gaardhøje, *ibid.* **42**, 483 (1992).
[6] A. Maj *et al.*, Acta Phys. Pol. B **26**, 417 (1995).
[7] N. Tsoneva, Ch. Stoyanov, Yu. P. Gangrsky, V. Yu. Ponomarev, N. P. Balabanov, and A. P. Tonchev, Phys. Rev. C **61**, 044303 (2000).
[8] I. Diószegi, I. Mazumdar, N. P. Shaw, and P. Paul, Phys. Rev. C **63**, 047601 (2001).
[9] S. K. Rathi, D. R. Chakrabarty, V. M. Datar, S. Kumar, E. T. Mirgule, A. Mitra, V. Nanal, and H. H. Oza, Phys. Rev. C **67**, 024603 (2003).
[10] N. D. Dang, K. Tanabe, and A. Arima, Phys. Lett. B **445**, 1 (1998); Nucl. Phys. **A645**, 536 (1999).
[11] V. Baran, M. Colonna, M. Di Toro, A. Guarnera, V. N. Kondratyev, and A. Smerzi, Nucl. Phys. **A599**, 29 (1996).
[12] M. Gallardo, M. Diebel, T. Døssing, and R. A. Broglia, Nucl. Phys. **A443**, 415 (1985).
[13] Y. Alhassid, Nucl. Phys. **A649**, 107c (1999), and references therein.
[14] W. E. Ormand, P. G. Bortignon, and R. A. Broglia, Nucl. Phys. **A614**, 217 (1997).
[15] W. E. Ormand, Nucl. Phys. **A649**, 145c (1999), and references therein.
[16] G. Shanmugam and V. Selvam, Phys. Rev. C **62**, 014302 (2000).
[17] G. Shanmugam and M. Thiagasundaram, Phys. Rev. C **37**, 853 (1988).
[18] G. Shanmugam and M. Thiagasundaram, Phys. Rev. C **39**, 1623 (1989).
[19] Y. Alhassid and B. Bush, Nucl. Phys. **A549**, 12 (1992).
[20] P. Arumugam, G. Shanmugam, and S. K. Patra, nucl-th/0401020.
[21] V. M. Strutinsky, Nucl. Phys. **A95**, 420 (1967); **A122**, 1 (1968).
[22] M. Brack, J. Damgaard, A. S. Jensen, H. C. Pauli, V. M. Strutinsky, and C.Y. Wong, Rev. Mod. Phys. **44**, 320 (1972).
[23] M. Bolsterli, E. D. Fiset, J. R. Nix, and J. L. Norton, Phys. Rev. C **5**, 1050 (1972).
[24] K. Neergård, V. V. Pashkevich, and S. Frauendorf, Nucl. Phys. **A262**, 61 (1976).
[25] S. Cohen, F. Plasil, and W. Swiatecki, Ann. Phys. (N.Y.) **82**, 557 (1974).
[26] G Shanmugam, V. Ramasubramanian, and S. N. Chintalapudi, Phys. Rev. C **63**, 064311 (2001).
[27] G. Shanmugam, P. R. Subramanian, M. Rajasekaran, and V. Devanathan, in *Proceedings of the International Conference on Nuclear Interactions*, Canberra, Australia, 1978, edited by B. A. Robson, Lecture Notes in Physics Vol. 92 (Springer, Heidelberg, 1979), p. 433.
[28] G. Shanmugam and P. Arumugam, Pramana, J. Phys. **57**, 223 (2001).
[29] M. Brack and P. Quentin, Nucl. Phys. **A361**, 35 (1981).
[30] O. Civitarese, A. L. De Paoli, and A. Plastino, Z. Phys. A **309**, 177 (1982); **311**, 317 (1983).
[31] A. V. Ignatyuk, I. N. Mikhailov, L. H. Molina, R. G. Nazmitdinov, and K. Pomorsky, Nucl. Phys. **A346**, 191 (1980).
[32] V. S. Ramamurthy, S. S. Kapoor, and S. K. Kataria, Phys. Rev. Lett. **25**, 386 (1970).
[33] R. R. Hilton, Z. Phys. A **309**, 233 (1983).
[34] P. Carlos, R. Bergere, H. Beil, A. Lepretre, and A. Veyssiere, Nucl. Phys. **A219**, 61 (1974).
[35] Y. Alhassid and B. Bush, Nucl. Phys. **A509**, 461 (1990).
[36] Y. Alhassid and B. Bush, Nucl. Phys. **A531**, 39 (1991).
[37] S. Levit and Y. Alhassid, Nucl. Phys. **A413**, 439 (1984).
[38] G. Shanmugam, K. Sankar, and K. Ramamurthy, Phys. Rev. C **52**, 1443 (1995).
[39] J. Gundlach, K. A. Snover, J. A. Behr, C. A. Gossett, M. K. Habior, and K. T. Lesko, Phys. Rev. Lett. **65**, 2523 (1990).
[40] D. Kusnezov, Y. Alhassid, and K. A. Snover, Phys. Rev. Lett. **81**, 542 (1998).
[41] T. Baumann *et al.*, Nucl. Phys. **A635**, 428 (1998).
[42] M. P. Kelly, K. A. Snover, J. P.S. van Schagen, K. Kicinska-Habior, and Z. Trznadel, Phys. Rev. Lett. **82**, 3404 (1999).
[43] M. Kicinska Habior, K. A. Snover, S. A. Behr, C. A. Gossett, Y. Alhassid, and N. Whelan, Phys. Lett. B **308**, 225 (1993).
[44] Y. Alhassid and N. Whelan, Nucl. Phys. **A565**, 427 (1993).
[45] B. Herskind *et al.*, Acta Phys. Pol. B **34**, 2467 (2003).
[46] A. Maj, Acta Phys. Pol. B **32**, 793 (2001).
[47] G. Shanmugam, P. Arumugam, and V. Ramasubramanian, in *Proceedings of the DAE Symposium on Nuclear Physics*, Mumbai, India, 1998, Vol. 41B, p. 100.